Waves Random Media 10 (2000) 17–31. Printed in the UK PII: S0959-7174(00)99501-6

Rough surface Green's function based on the first-order modified perturbation and smoothed diagram methods

Akira Ishimaru, John D Rockway and Yasuo Kuga

Department of Electrical Engineering, University of Washington, Box 352500, Seattle, WA 98195-2500, USA

E-mail: ishimaru@ee.washington.edu

Received 20 November 1998, in final form 16 July 1999

Abstract. This paper presents an analytical theory of rough surface Green's functions based on the extension of the diagram method of Bass, Fuks, and Ito with the smoothing approximation used by Watson and Keller. The method is a modification of the perturbation method and is applicable to rough surfaces with small RMS height. But the range of validity is considerably greater than for the conventional perturbation solutions. We consider one-dimensional rough surfaces with a Dirichlet boundary condition. The coherent Green's function is obtained from the smoothed Dyson's equation using a spatial Fourier transform. The mutual coherence function for the Green's function is obtained by first-order iteration of the smoothing approximation applied to the Bethe–Salpeter equation in terms of a quadruple Fourier transform. These integrals are evaluated by the saddle-point technique. The equivalent bistatic cross section per unit length of the surface is compared with that for the conventional perturbation method and the Watson–Keller result. With respect to the Watson–Keller result, it should be noted that our result is reciprocal, while the Watson–Keller result is non-reciprocal. Included in this paper is a discussion of the specific intensity at a given observation point. The theory developed will be useful for RCS signature related problems and low grazing angle scattering when both the transmitter and the object are close to the surface.

1. Introduction

Extensive studies of the rough surface scattering problem have been made. Most studies deal with plane wave incidence and the scattering characteristics are expressed in terms of the cross sections per unit area of the rough surface [1–3]. While this is appropriate for moderate angles of incidence (less then 75°), the assumption of plane wave incidence is no longer appropriate when the transmitter and target are near the ocean surface or for low grazing angle (LGA) scattering. For larger angles of incidence, and scattering near the surface, careful examination of the plane wave assumption is required. For LGA scattering, it has already been pointed out by Barrick [4] that 'propagation and scatter become inextricably connected' and 'the free-space plane wave description may not suffice'. The wave incident at a point on a rough surface is not the direct plane or spherical wave from the transmitter. The incident wave is modified by the rough surface itself. The incident wave at a point on the rough surface is a sum of the free-space plane wave from the transmitter and the scattered wave from the surface. In this paper, we consider the radiation from a point source located at any point near the rough surface, and thus the field on the surface is the total field.

In recent years, several numerical Monte Carlo techniques have been developed to obtain numerical solutions to the rough surface scattering problem [5]. While this is an excellent

0959-7174/00/010017+15$30.00

approach to the study of rough surface scattering, when the grazing angle becomes small, extremely large surface areas are required to take proper account of the large footprint area. Thus fast, high-performance computers are required for solutions. The rough surface Green's function is analytical, and the computer requirement is reduced. Fast analysis of the rough surface effects is possible. This is important when considering problems in which the rough surface correction of scattering from near-surface objects must be included.

In this paper, we present an analytical theory of the rough surface Green's function for a one-dimensional Dirichlet rough surface. This provides a mathematically simple formulation including the effects of rough surfaces, but it does not include cross-polarization effects. We begin with Green's theorem, and using an equivalent boundary condition, we obtain Dyson's equation for the coherent field which is obtained using a spatial Fourier transform. Since the surface is Dirichlet, the equivalent impedance is zero for the flat surface. However, the impedance is not zero due to the presence of roughness. Moreover, corresponding to this impedance, there exist surface wave poles, giving rise to surface wave propagation along the surface.

The coherent field case is shown to be equivalent to the Watson–Keller results. Next, we examine the Bethe–Salpeter equation and obtain the first-order iteration solution, once again making use of the spatial Fourier transform. The cross section per unit length is calculated and is shown to be similar to the Watson–Keller result; but, more importantly, it is reciprocal. Discussions are also included on power conservation and the specific intensity. This paper discusses the first-order modified perturbation theory of the rough surface Green's function and the far-field approximation. In the future, we shall discuss the surface wave contributions applicable to the LGA case and the second-order modified perturbation techniques which extend the range of validity of this theory. Section 2 discusses the coherent Green's function and the equivalent surface impedance. Section 3 discusses the incoherent Green's function and asymptotic solutions. Sections 4 and 5 discuss the surface cross sections and the specific intensity.

2. Coherent rough surface Green's function

In this section, we present Dyson's equation which is the integral equation for the coherent Green's function [3, 6]. We make use of the smoothing approximation [7, 8] and the spatial Fourier transform to obtain the coherent Green's function $\langle G(r, r_0)\rangle$. Asymptotic forms for the far fields are obtained using the saddle-point technique.

2.1. First-order smoothed Dyson's equation

We derive the fundamental Dyson's equation which will be used in describing the rough surface Green's function using Green's theorem [3, 6–9]. This is a nonlinear equation for the coherent Green's function. To simplify the problem, a first-order smoothing operation is applied to Dyson's equation making it linear. The Green's function for a given point source located at $r = r_0$ satisfies the equation

$$(\nabla^2 + k^2)G(r, r_0) = -\delta(r - r_0). \tag{1}$$

The Green's function must also satisfy the boundary conditions $G(r, r_0) = 0$ on the rough surface $z = h$. The rough surface is described by a surface profile $h(x)$ which is a random function of the surface height. We convert this boundary condition to an equivalent boundary condition at $z = 0$ by expanding the Green's function about the surface height $h(x)$. The

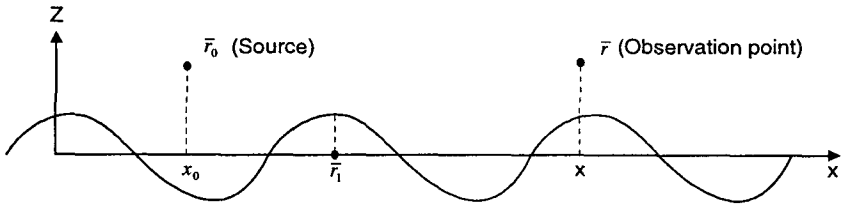

Figure 1. The rough surface is described by $h = h(x)$. The source point is at r_0 and the observation point is at r and r_1 is on the surface at $z = 0$.

boundary condition $G(r_s, r_0) = 0$ about $z = 0$ becomes

$$G(r_1, r_0) + h(x)\frac{\partial}{\partial z_1}G(r_1, r_0) + \frac{h^2(x)}{2}\frac{\partial^2}{\partial z_1^2}G(r_1, r_0) + \ldots = 0 \tag{2}$$

where r_1 is on the flat surface at $z = 0$. We keep the first-order term in h and the higher-order powers of h are neglected (figure 1). We now use Green's theorem

$$G(r, r_0) = G_0(r, r_0) + \int_S \left(G(r, r_1)\frac{\partial}{\partial n_1}G_0(r_1, r_0) - G_0(r, r_1)\frac{\partial}{\partial n_1}G(r_1, r_0) \right) \mathrm{d}s_1 \tag{3}$$

where $G_0(r, r_0)$ is the flat-surface Green's function satisfying the Dirichlet condition $G_0(r, r_0) = 0$ on the flat surface. Applying the equivalent boundary condition (2) to Green's theorem and making use of the flat-surface Green's function and its boundary condition, Green's theorem simplifies to

$$G(r, r_0) = G_0(r, r_0) + \int_S \left(-h(x_1)\frac{\partial}{\partial z_1}G(r_1, r_0) \right) \frac{\partial}{\partial z_1}G_0(r_1, r_0)\, \mathrm{d}x_1.$$

We rewrite this in terms of the random surface potential of the rough surface.

$$G(r, r_0) = G_0(r, r_0) + \int_S G_0(r_1, r_0)V(r_1)G(r_1, r_0)\, \mathrm{d}x_1 \tag{4}$$

where we define

$$V(r_1) = -\frac{\partial^{\leftarrow}}{\partial z_1}h(x_1)\frac{\partial^{\rightarrow}}{\partial z_1} \tag{5}$$

as the random surface potential [3] which is a function of the random surface height $h(x)$. The arrows on the derivatives indicate the direction in which the derivatives are operated. Starting with (4), we can obtain Dyson's equation for the average (coherent) Green's function $\langle G(r, r_0) \rangle$. It is derived using the diagram method [6]. Figure 2(*a*) shows Dyson's equation in diagrammatic form.

$$\langle G(r, r_0) \rangle = G_0(r, r_0) + \int G_0(r, r_2)M(r_2, r_1)\langle G(r_1, r_0) \rangle\, \mathrm{d}x_1\, \mathrm{d}x_2 \tag{6}$$

and M is called the mass operator.

Note that equation (6) applies to any point r, above the surface at $z = 0$. As r approaches the flat surface, $G_0(r, r_0)$ becomes zero, but $G_0(r, r_0)$ inside the integral is not zero, because M includes the derivative $\partial/\partial z$. In addition, note that $\langle G(r, r_0) \rangle$ is not zero on the flat surface. Dyson's equation is a nonlinear equation for the coherent Green's function. To simplify Dyson's equation, the mass operator may be approximated using the first-order smoothing operation or the 'Bourret approximation'. This approximation is also called the 'smoothing first-order' approximation [6]. Figure 2(*b*) shows Dyson's equation using the first-order smoothing in diagrammatic form.

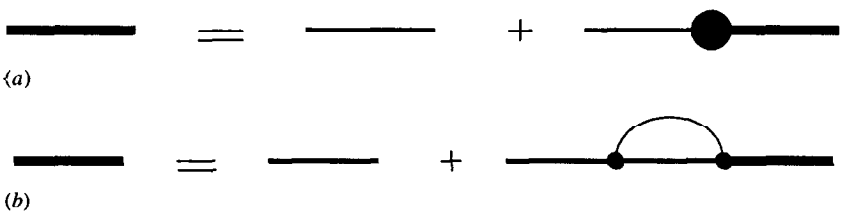

(*a*)

(*b*)

Figure 2. (*a*) Diagrammatic form of the nonlinear Dyson's equation for the coherent Green's function. (*b*) Dyson's equation with smoothing approximation.

The mass operator under this approximation is given by

$$M(r_2, r_1) = \langle V(r_2)V(r_1)\rangle G_0(r_2, r_1). \tag{7}$$

Rewriting the expression for the first-order smoothing mass operator, we have

$$\begin{aligned} M(r_2, r_1) &= \langle V(r_2)V(r_1)\rangle G_0(r_2, r_1) = \langle V(r_2)G_0(r_2, r_1)V(r_1)\rangle \\ &= \left\langle \frac{\partial^{\leftarrow}}{\partial z_2} h(x_2) \frac{\partial^{\rightarrow}}{\partial z_2} G_0(r_2, r_1) \frac{\partial^{\leftarrow}}{\partial z_1} h(x_1) \frac{\partial^{\rightarrow}}{\partial z_1} \right\rangle \\ &= \frac{\partial^{\leftarrow}}{\partial z_2} \frac{\partial^2}{\partial z_2 \partial z_1} G_0(r_2, r_1) \langle h(x_2)h(x_1)\rangle \frac{\partial^{\rightarrow}}{\partial z_1}. \end{aligned} \tag{8}$$

Dyson's equation then becomes

$$\langle G(r, r_0)\rangle = G_0(r, r_0) + \int G_0(r, r_2)\langle V(r_2)G_0(r_2, r_1)V(r_1)\rangle \langle G(r_1, r_0)\rangle \, dx_1 \, dx_2. \tag{9}$$

Thus, we must solve Dyson's equation (9) for the given mass operator (8) under the first-order smoothing operation.

2.2. *Dyson's equation in spatial Fourier transform representation*

We first rewrite Dyson's equation (9) explicitly

$$\begin{aligned} \langle G(r, r_0)\rangle &= G_0(r, r_0) \\ &\quad + \int \frac{\partial}{\partial z_2} G_0(r, r_2) \frac{\partial^2}{\partial z_1 z_2} G_0(r_2, r_1) \langle h(r_2)h(r_1)\rangle \frac{\partial}{\partial z_1} \langle G(r_1, r_0)\rangle \, dx_1 \, dx_2. \end{aligned} \tag{10}$$

To solve Dyson's equation for the coherent Green's function, we make use of a spatial Fourier transform representation. The flat-surface Green's function is then given by

$$G_0(r, r_0) = \frac{1}{2\pi} \int G_0(\kappa; z, z_0) e^{i\kappa(x - x_0)} \, d\kappa. \tag{11}$$

We also note the following expressions in Dyson's equation. We define the variables and the corresponding spatial Fourier transform pair for the derivatives of the Green's functions:

$$\begin{aligned} A(r, r_2) &= G_0(r, r_2) \frac{\partial^{\leftarrow}}{\partial z_2} \quad &&\Rightarrow A(\kappa; z, z_2) = G_0(\kappa; z, z_2) \frac{\partial^{\leftarrow}}{\partial z_2} \\ B(r_2, r_1) &= \frac{\partial^2}{\partial z_2 \partial z_1} G_0(r_2, r_1) &&\Rightarrow B(\kappa; z_2, z_1) = \frac{\partial^2}{\partial z_2 \partial z_1} G_0(\kappa; z_2, z_1) \\ C(r_1, r_0) &= \frac{\partial}{\partial z_1} \langle G(r_1, r_0)\rangle &&\Rightarrow C(\kappa, z_1, z_0) = \frac{\partial^{\rightarrow}}{\partial z_1} \langle G(\kappa; z_1, z_0)\rangle. \end{aligned} \tag{12}$$

Inserting these elements into Dyson's equation and taking the spatial Fourier transform we obtain

$$\frac{1}{2\pi}\int \langle G(\kappa; z, z_0)\rangle e^{i\kappa(x-x_0)}\,d\kappa = \frac{1}{2\pi}\int G_0(\kappa; z, z_0)e^{i\kappa(x-x_0)}\,d\kappa + \int dx_1\,dx_2 \frac{1}{2\pi}\int A(\kappa; z, z_2)e^{i\kappa(x-x_2)}\,d\kappa \frac{1}{2\pi}\int e^{i\kappa'(x_2-x_1)}\,B(\kappa'; z_2, z_1)d\kappa' \times \int e^{i\kappa''(x_2-x_1)}W(\kappa'')\,d\kappa'' \frac{1}{2\pi}\int e^{i\kappa'''(x_1-x_0)}C(\kappa'''; z_1, z_0)\,d\kappa''' \tag{13}$$

where the surface height correlation is given by the spatial Fourier transform of the spectral density $W(\kappa)$,

$$\langle h(r_1)h(r_2)\rangle = \int W(\kappa)e^{i\kappa(x_2-x_1)}\,d\kappa. \tag{14}$$

The integrals over the surface $dx_1\,dx_2$ may be simplified by noticing the following relationship:

$$\int dx_1 = 2\pi\delta(-\kappa' - \kappa'' + \kappa''') \qquad \int dx_2 = 2\pi\delta(-\kappa + \kappa' + \kappa''). \tag{15}$$

This implies that the integrals in the spatial frequency can be integrated.

$$\int d\kappa''' \to \kappa''' = \kappa' + \kappa'' = \kappa \qquad \int d\kappa'' \to \kappa'' = \kappa - \kappa'. \tag{16}$$

Making use of these integral identities, and removing the common

$$\frac{1}{2\pi}\int e^{i\kappa(x-x_0)}\,d\kappa$$

we simplify and obtain the spatial Fourier transform representation of Dyson's equation.

$$\langle G(\kappa; z, z_0)\rangle = G_0(\kappa; z, z_0) + A(\kappa)C(\kappa)\int B(\kappa')W(\kappa - \kappa')d\kappa'. \tag{17}$$

For a point source, the flat-space Green's function is given by:

$$G_0(r, r_0) = \frac{1}{2\pi}\int \frac{i}{2k_z}\left[e^{ik_z|z-z_0|} - e^{ik_z(z+z_0)}\right]e^{i\kappa(x-x_0)}\,d\kappa. \tag{18}$$

Then, the spatial Fourier transform representation is:

$$G_0(\kappa; z, z_0) = \frac{i}{2k_z}\left[e^{ik_z|z-z_0|} - e^{ik_z(z+z_0)}\right]. \tag{19}$$

Likewise, the spatial Fourier transform representation of the coherent Green's function may be written in a similar manner,

$$\langle G(\kappa; z, z_0)\rangle = \frac{i}{2k_z}\left[e^{ik_z|z-z_0|} + R(\kappa)e^{ik_z(z+z_0)}\right]. \tag{20}$$

Inserting (19) and (20) into (17), we arrive at a solution for the reflection coefficient,

$$R(\kappa) + 1 = k_z(1 - R(\kappa))\int k_z' W(\kappa - \kappa')\,d\kappa'. \tag{21}$$

The reflection coefficient for the rough surface is therefore given by:

$$R(\kappa) = \frac{Q-1}{Q+1} \qquad \text{where} \qquad Q(\kappa) = k_z\int k_z' W(\kappa - \kappa')\,d\kappa'. \tag{22}$$

Therefore, the coherent rough surface Green's function is given below where the reflection coefficient is given by (22),

$$\langle G(r, r_0)\rangle = \frac{1}{2\pi}\int \frac{\mathrm{i}}{2k_z}\left[\mathrm{e}^{\mathrm{i}k_z|z-z_0|} + R(\kappa)\mathrm{e}^{\mathrm{i}k_z(z+z_0)}\right]\mathrm{e}^{\mathrm{i}\kappa(x-x_0)}\,\mathrm{d}\kappa. \tag{23}$$

The integrand contains the reflection coefficient $R(\kappa)$ which has a pole at $Q(\kappa) = -1$. This pole gives rise to surface wave contributions from the rough surface. If we evaluate the residue for equation (23), this represents the surface wave similar to the Sommerfeld dipole problem.

Note that the coherent Green's function is given in the spatial Fourier transform representation. The evaluation of this integral will be performed using the saddle-point technique.

2.3. Asymptotic form of the coherent Green's function

Let us examine the coherent Green's function given in (23). The coherent element in the Green's function consists of three terms: the direct wave generated from the point source, the unperturbed reflected wave from a smooth surface, and the coherent reflection from a perturbed surface which was constructed from the stochastic process (figure 3). We wish to evaluate each term in the far field, for $kR \to \infty$, so that the saddle-point asymptotic technique may be used. The direct wave can be shown to be the following [10],

$$\langle G(r, r_0)\rangle_{\text{direct}} = \frac{1}{2\pi}\int \frac{\mathrm{i}}{2k_z(\kappa)}\left(\mathrm{e}^{\mathrm{i}\kappa x + \mathrm{i}k_z|z-z_0|}\right)\mathrm{d}\kappa = \frac{\mathrm{i}}{4}H_0^{(1)}(kR_0)$$
$$\approx \frac{\mathrm{i}}{4}\sqrt{\frac{2}{\pi k R_0}}\,\mathrm{e}^{\mathrm{i}kR_0 - \mathrm{i}\pi/4} \tag{24}$$

where the last expression is the asymptotic form in the far field for large kR_0.

Next, we examine the second term in (23). Evaluation of the integral must be done carefully due to the presence of the pole contained within the reflection coefficient. The second term, representing reflection from the rough surface, can be evaluated for large kR_0 using the modified

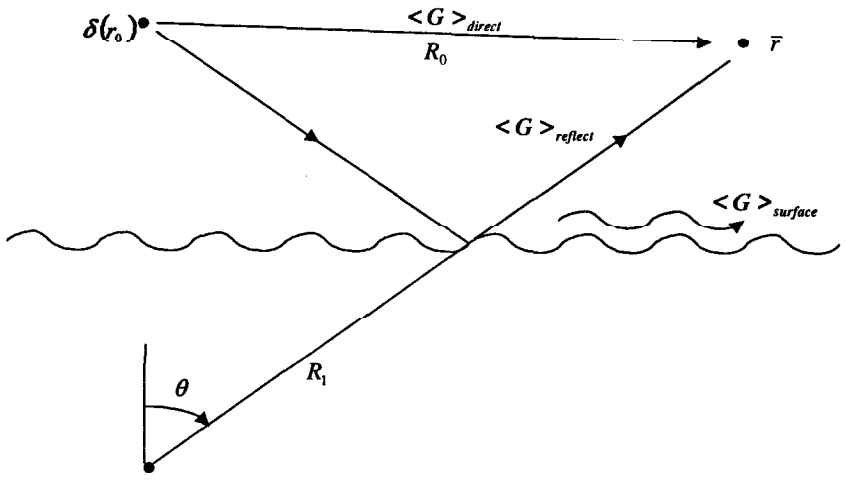

Figure 3. The coherent Green's function $\langle G\rangle$ consists of the direct field $\langle G\rangle_{direct}$, the far field from the image $\langle G\rangle_{\text{reflect}}$, and the surface wave contributions $\langle G\rangle_{\text{surface}}$.

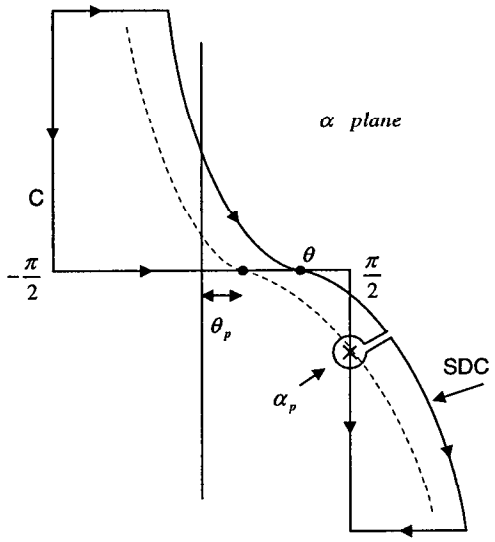

Figure 4. Original contour of integration C, steepest descent contour (SDC), and the location of the pole α_p.

saddle-point technique, taking into account the presence of the pole [10]. Here, however, we give a simplified approximate evaluation. We make use of the transformation

$$z = R\cos\theta \qquad x = R\sin\theta \qquad \kappa = k\sin\alpha \qquad k_z = \sqrt{k^2 - \kappa^2} = k\cos\alpha.$$

The contour of integration along the path of steepest descent (SDC) is shown in figure 4. The saddle-point is at $\alpha = \theta$, and θ_p is the saddle-point when the SDC goes through the pole at α_p. Therefore, the integral (23) is given approximately by

$$\langle G\rangle = \begin{cases} \langle G\rangle_{\text{direct}} + \langle G\rangle_{\text{reflected}} & \text{if } \theta < \theta_p \\ \langle G\rangle_{\text{direct}} + \langle G\rangle_{\text{reflected}} + \langle G\rangle_{\text{surface}} & \text{if } \theta > \theta_p. \end{cases} \tag{25}$$

The saddle-point evaluation of the reflected wave $\langle G\rangle_{\text{reflected}}$ is given by

$$\langle G(\boldsymbol{r}, \boldsymbol{r}_0)\rangle_{\text{reflected}} \approx \frac{\mathrm{i}}{4}\sqrt{\frac{2}{\pi k R_1}}\,\mathrm{e}^{\mathrm{i}kR_1 - \mathrm{i}\pi/4} R(k\sin\theta). \tag{26}$$

The surface wave term $\langle G\rangle_{\text{surface}}$ is given by the residue evaluation [10],

$$\begin{aligned}\langle G\rangle_{\text{surface}} &= 2\pi\mathrm{i} \times (\text{residue at } \alpha_p) \\ &= \frac{1}{k_{zp}(\partial Q/\partial\kappa)_{\kappa_p}} \exp\left[\mathrm{i}k_{zp}(z + z_0) + \mathrm{i}\kappa_p(x - x_0)\right]\end{aligned} \tag{27}$$

where κ_p is the root of $Q(\kappa_p) + 1 = 0$.

2.4. Equivalent surface impedance

Let us consider the reflection coefficient $R(\kappa)$ given in (22). This is identical to the reflection coefficient given by Watson–Keller and can also be compared with the field perturbation R_{fp} and the phase perturbation R_{pp} methods [11]:

$$R_{Ish}(\kappa) = \frac{Q-1}{Q+1} \qquad R_{fp} = -1 + 2Q \qquad R_{pp} = -\mathrm{e}^{-2Q}. \tag{28}$$

We also note that we can express the reflection coefficient in terms of the surface impedance Z_s. The wave impedance for an acoustic or horizontally polarized electromagnetic wave obliquely incident on a surface is given by

$$Z_1 = Z_0 \frac{k}{k_z} \tag{29}$$

where Z_0 is the characteristic impedance of the medium. Therefore, we write

$$R = \frac{Z_s - Z_1}{Z_s + Z_1} \tag{30}$$

where the surface impedance Z_s is given by

$$Z_s = Z_0 \frac{k}{k_z} Q. \tag{31}$$

Note that the equivalent surface impedance of the rough surface is not zero, even though the surface impedance for a flat Dirichlet surface is zero.

3. Incoherent rough surface Green's function

In this section, we present the Bethe–Salpeter equation which will yield the integral equation describing the second moment of the Green's function. The second moment is also called the mutual coherence function, and gives the spatial correlation and the angular spectra of the incoherent field. The first-order iteration is applied to the Bethe–Salpeter equation yielding a fifth-order integral. Using asymptotic approximations these integrals are evaluated. Our first-order incoherent intensity is then compared with the existing first-order perturbation and the Watson–Keller result.

3.1. First-order Bethe–Salpeter equation

The rough surface Green's function G is given by the sum of the coherent $\langle G \rangle$ and the incoherent (fluctuating) G_f Green's function,

$$G(\boldsymbol{r}, \boldsymbol{r}_0) = \langle G(\boldsymbol{r}, \boldsymbol{r}_0) \rangle + G_f. \tag{32}$$

To obtain the fluctuating Green's function we must consider the second moment,

$$\Gamma(\boldsymbol{r}, \boldsymbol{r}'; \boldsymbol{r}_0, \boldsymbol{r}_0') = \left\langle G(\boldsymbol{r}, \boldsymbol{r}_0) G^*(\boldsymbol{r}', \boldsymbol{r}_0') \right\rangle. \tag{33}$$

Noting (32), the mutual coherence function is given by

$$\Gamma = \Gamma_0 + \Gamma_f \tag{34}$$

where the coherent mutual coherence function is given by

$$\Gamma_0 = \langle G(\boldsymbol{r}, \boldsymbol{r}_0) \rangle \left\langle G^*(\boldsymbol{r}', \boldsymbol{r}_0') \right\rangle \tag{35}$$

which was determined in section 2. The fluctuating or incoherent mutual coherence function

$$\Gamma_f = \left\langle G_f(\boldsymbol{r}, \boldsymbol{r}_0) G_f^*(\boldsymbol{r}', \boldsymbol{r}_0') \right\rangle \tag{36}$$

is now considered. The second moment Γ satisfies the following Bethe–Salpeter equation under the smoothing approximation [6].

$$\left\langle G(\boldsymbol{r}, \boldsymbol{r}_0) G^*(\boldsymbol{r}', \boldsymbol{r}_0') \right\rangle = \langle G(\boldsymbol{r}, \boldsymbol{r}_0) \rangle \left\langle G^*(\boldsymbol{r}', \boldsymbol{r}_0') \right\rangle + \int d\boldsymbol{r}_1 \, d\boldsymbol{r}_1' \langle G(\boldsymbol{r}, \boldsymbol{r}_1) \rangle \left\langle G^*(\boldsymbol{r}', \boldsymbol{r}_1') \right\rangle \left\langle V(\boldsymbol{r}_1) V(\boldsymbol{r}_1') \right\rangle \left\langle G(\boldsymbol{r}_1, \boldsymbol{r}_0) G^*(\boldsymbol{r}_1', \boldsymbol{r}_0') \right\rangle \tag{37}$$

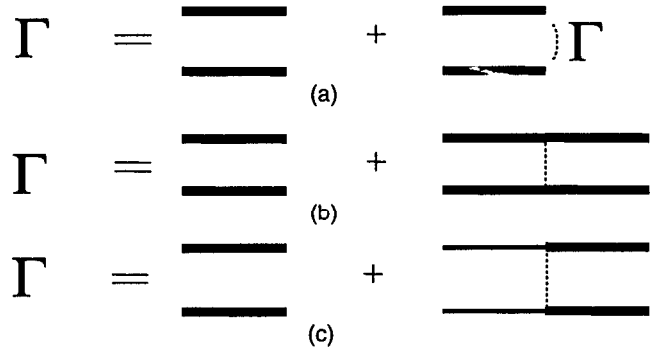

Figure 5. Approximation comparisons of the Bethe–Salpeter equation in diagrammatic representation. (*a*) Smoothed Bethe–Salpeter equation. (*b*) Ishimaru's first-order solution. (*c*) Ito's first-order solutions in diagrammatic form.

where

$$\langle V(r_1)V(r_1')\rangle = \left\langle \frac{\partial^{\leftarrow}}{\partial z_1} h(x_1) \frac{\partial^{\rightarrow}}{\partial z_1} \frac{\partial^{\leftarrow}}{\partial z_1'} h(x_1') \frac{\partial^{\rightarrow}}{\partial z_1'} \right\rangle. \tag{38}$$

A diagrammatic representation of (37) is given in figure 5(*a*). We now consider the first-order iteration shown in figure 5(*b*). The incoherent part of the mutual coherence function Γ_f is therefore given by

$$\Gamma_f = \int dr_1\, dr_1' \langle G(r, r_1)\rangle \langle G^*(r', r_1')\rangle \langle V(r_1)V(r_1')\rangle \langle G(r_1, r_0)\rangle \langle G^*(r_1', r_0')\rangle. \tag{39}$$

Noting (38), the incoherent mutual coherence function is given explicitly by

$$\Gamma_f = \int dr_1\, dr_1' \frac{\partial}{\partial z_1}\langle G(r, r_1)\rangle \frac{\partial}{\partial z_1'} \langle G^*(r', r_1')\rangle \langle h(x_1)h(x_1')\rangle \times \frac{\partial}{\partial z_1}\langle G(r_1, r_0)\rangle \frac{\partial}{\partial z_1'} \langle G^*(r_1', r_0')\rangle. \tag{40}$$

To solve the first-order Bethe–Salpeter equation using the first-order iteration, we once again make use of the spatial Fourier transform.

$$\langle G(r, r_1)\rangle = \frac{1}{2\pi} \int d\kappa \frac{i}{2k_z} \left(e^{ik_z|z-z_1|} + R(\kappa)e^{ik_z(z+z_1)}\right) e^{i\kappa(x-x_1)}. \tag{41}$$

Substituting the coherent Green's function (41) into (39), we arrive at the spatial Fourier transform representation of the Bethe–Salpeter equation.

$$\Gamma_f = \int dx_1\, dx_1' \frac{1}{2\pi} \int d\kappa A(\kappa) e^{i\kappa(x-x_1)} \left(\frac{1}{2\pi} \int d\kappa' A'(\kappa') e^{i\kappa'(x'-x_1')}\right)^* \times \frac{1}{2\pi} \int d\kappa_2 W(\kappa_2) e^{i\kappa_2(x_1-x_1')} \frac{1}{2\pi} \int d\kappa_1 B(\kappa_1) e^{i\kappa_1(x_1-x_0)} \times \left(\frac{1}{2\pi} \int d\kappa_1' B'(\kappa_1') e^{i\kappa_1'(x_1'-x_0')}\right)^* \tag{42}$$

where the elements in the integral are obtained from the derivatives of the coherent Green's function in (40),

$$A(\kappa) = \frac{1 - R(\kappa)}{2} e^{ik_z z} \qquad B(\kappa_1) = \frac{1 - R(\kappa_1)}{2} e^{ik_{z1} z_0}$$
$$A'(\kappa') = \frac{1 - R(\kappa')}{2} e^{ik_z' z'} \qquad B(\kappa_1') = \frac{1 - R(\kappa_1')}{2} e^{ik_{z1}' z_0'}. \tag{43}$$

To simplify the integrals, we make a coordinate transformation. First, note that the exponential may be written as:

$$\exp\{-i\kappa x_1 + i\kappa' x_1'\} = \exp\{-i\kappa_c x_{1d} - i\kappa_d x_{1c}\}$$

where

$$\kappa_c = \frac{\kappa + \kappa'}{2} \qquad \kappa_d = \kappa - \kappa' \qquad x_{1d} = x_1 - x_1' \qquad x_{1c} = \frac{x_1 + x_1'}{2}$$

also $\exp\{i\kappa_2(x_1 - x_1')\} = \exp\{i\kappa_2 x_{1d}\}$ and, finally,

$$\exp\{i\kappa_1 x_1 - i\kappa_1' x_1'\} = \exp\{i\kappa_{1c} x_{1d} + i\kappa_{1d} x_{1c}\}$$

where

$$\kappa_{1c} = \frac{\kappa_1 + \kappa_1'}{2} \qquad \kappa_{1d} = \kappa_1 - \kappa_1'.$$

Using these transformations and noting that $dx_1\, dx_1' = dx_{1c} dx_{1d}$, we can simplify (41) by integrating over dx_{1d} and $d\kappa_2$. This yields

$$\int dx_{1d} \to 2\pi\delta(-\kappa_c + \kappa_2 + \kappa_{1c}) \qquad \int d\kappa_2 \to \kappa_2 = \kappa_c - \kappa_{1c}. \tag{44}$$

This simplifies the integral for the first-order incoherent mutual coherence function to a coupled fifth-order integral.

$$\begin{aligned}\Gamma_f = 2\pi \int dx_{1c} \frac{1}{2\pi} \int d\kappa \frac{1 - R(\kappa)}{2} \exp[ik_z z + i\kappa(x - x_{1c})] \\ \times \left(\frac{1}{2\pi} \int d\kappa' \frac{1 - R(\kappa')}{2} \exp[ik_z' z' + i\kappa'(x' - x_{1c})]\right)^* W\left(\frac{\kappa + \kappa'}{2} - \frac{\kappa_1 + \kappa_1'}{2}\right) \\ \times \frac{1}{2\pi} \int d\kappa_1 \frac{1 - R(\kappa_1)}{2} \exp[ik_{z1} z_0 + i\kappa_1(x_{1c} - x_0)] \\ \times \left(\frac{1}{2\pi} \int d\kappa_1' \frac{1 - R(\kappa_1')}{2} \exp[ik_{z1}' z_0' + i\kappa_1'(x_{1c} - x_0')]\right)^*. \end{aligned} \tag{45}$$

This is the mutual coherence function of the first-order incoherent Green's function expressed in a quadruple spatial Fourier transform representation. These Fourier transforms are evaluated approximately by the saddle-point technique discussed in the next section.

3.2. Asymptotic solution for the incoherent mutual coherence function Γ_f

For the incoherent field the second moment is given by expression (45). It involves the integration of five integrals which are coupled together. We approximate the coupled integrals by a far-field, asymptotic approximation in which each of the integrals decouple.

In equation (45), the surface spectrum W is a function of $\kappa, \kappa', \kappa_1$ and κ_1' which, in general, vary from $-\infty$ to $+\infty$. However, under the far-field approximation, only certain values of $\kappa, \kappa', \kappa_1$ and κ_1' satisfy the geometric angular relationship shown in figure 6. Under this condition, W is evaluated only at the angles

$$\kappa = k\sin\theta_1 \quad \kappa' = k\sin\theta_1' \qquad \kappa_1 = k\sin\theta_2 \quad \kappa_1' = k\sin\theta_2'.$$

First, we note that

$$\frac{1 - R(\kappa)}{2} = \frac{1}{Q(\kappa) + 1}. \tag{46}$$

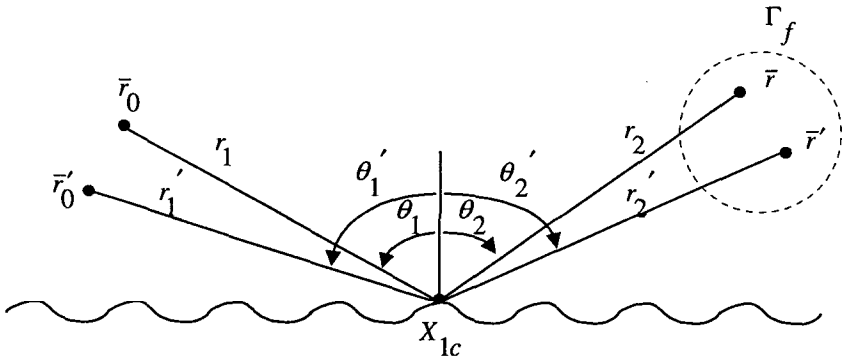

Figure 6. Incoherent mutual coherent function.

Then, following the asymptotic technique developed in section 2.3, each of the spatial transform integrals may be evaluated as

$$\begin{aligned} F(r,\theta) &= \frac{1}{2\pi}\int \mathrm{d}\kappa \frac{1-R(\kappa)}{2}\exp\{\mathrm{i}k_z z + \mathrm{i}\kappa x\} \\ &\approx \frac{1}{2\pi}\frac{1}{Q(k\sin\theta)+1}k\cos\theta\sqrt{\frac{2\pi}{kr}}\exp\left\{\mathrm{i}kr - \mathrm{i}\frac{\pi}{4}\right\} \\ &\approx \frac{-2\mathrm{i}k\cos\theta}{Q(k\sin\theta)+1}g_0(r) \end{aligned} \tag{47}$$

where

$$g_0(r) = \frac{\mathrm{i}}{4}\sqrt{\frac{2}{\pi kr}}\exp\left\{\mathrm{i}kr - \mathrm{i}\frac{\pi}{4}\right\}$$

is the free-space Green's function.

Therefore, using the saddle-point evaluation of Γ_f, we can express the incoherent mutual coherence function $\Gamma(r, r_0)$ in the approximate form

$$\Gamma_f(r,r';r_0,r_0') = 2\pi\int \mathrm{d}x_{1c}F(r_2\theta_2)F^*(r_2'\theta_2')W(\theta_2,\theta_2',\theta_1,\theta_1')F(r_1,\theta_1)F^*(r_1',\theta_1') \tag{48}$$

where $F(r,\theta)$ is given by expression (47) and

$$W = W\left(\frac{k\sin\theta_2 + k\sin\theta_2'}{2} - \frac{k\sin\theta_1 + k\sin\theta_1'}{2}\right). \tag{49}$$

The radial and angular variables for the mutual coherence function are shown in figure 6.

4. Cross section per unit length and conservation of power

Let us first consider the coherent field $\langle G\rangle$ which consists of the direct wave $\langle G\rangle_{\text{direct}}$ and the reflected field $\langle G\rangle_{\text{reflected}}$. We now consider the incoherent field. We express the mutual coherence function Γ_f in (48) in the following form using the generalized cross section σ per unit length of the rough surface.

$$\Gamma(r,r';r_0,r_0') = \int \frac{\mathrm{d}x_{1c}}{2\pi}\frac{1}{(r_2r_2')^{1/2}}\mathrm{e}^{\mathrm{i}kr_2-\mathrm{i}kr_2'}\sigma^0\frac{1}{(r_1r_1')^{1/2}}\mathrm{e}^{\mathrm{i}kr_1-\mathrm{i}kr_1'} \tag{50}$$

where

$$\sigma = \frac{2\pi}{k}\frac{4(k\cos\theta_2)(k\cos\theta_2')(k\cos\theta_1)(k\cos\theta_1')}{(1+Q(\theta_2))(1+Q(\theta_2'))^*(1+Q(\theta_1))(1+Q(\theta_1'))^*}W(\kappa_c-\kappa_{1c}). \tag{51}$$

For $r_0' = r_0$, $\theta_2 = \theta_2'$ and $\theta_1 = \theta_1'$, the generalized cross section σ reduces to the bistatic cross section per unit length,

$$\sigma_{\text{Ish}}^0 = \frac{2\pi}{k} \frac{4k^2 \cos^2\theta_2 k^2 \cos^2\theta_1 W(\kappa_c - \kappa_{1c})}{|1 + Q(\theta_2)|^2 |1 + Q(\theta_1)|^2}. \tag{52}$$

This may be compared with the Watson–Keller formula [7, 8]

$$\sigma_{\text{WK}}^0 = \frac{2\pi}{k} \frac{4k^2 \cos^2\theta_2 k^2 \cos^2\theta_1 W(\kappa_c - \kappa_{1c})}{|1 + Q(\theta_1)|^2}. \tag{53}$$

Notice that our bistatic cross section σ^0 is reciprocal, while the Watson–Keller formula (53) is non-reciprocal. Physically, (52) means, as shown in figure 6, that a coherent wave including the rough surface effect as given in the reflection coefficient (23) is incident at the surface x_{1c}. The scattered wave then propagates from x_{1c} to the observation point also as a coherent wave including the rough surface effects. The Watson–Keller result (53), on the other hand, propagates an incident field that is also coherent. However, the scattered wave propagates in free space and does not include the rough surface effect. This is best seen in the difference between theories for Dyson's equation shown in figure 5. We also note that the cross section for the conventional perturbation solution is given by

$$\sigma_{\text{p}}^0 = \frac{2\pi}{k} 4k^2 \cos^2\theta_2 k^2 \cos^2\theta_1 W(k_c - k_{1c}). \tag{54}$$

The bistatic cross sections σ_{Ish}^0, σ_{WK}^0 and σ_{p}^0 are calculated and shown in figure 7 along with Monte Carlo numerical calculations of rough surface scattering. The numerical Monte Carlo simulations were conducted under 500 realizations. Note that for small RMS height $k\sigma \leqslant 0.25$, all three cross sections are approximately equivalent. As $k\sigma$ increases the field perturbation increases faster than the Watson–Keller and the Ishimaru cross section. Our first-order solutions are below the exact numerical values, and it is expected that the higher-order solutions will add power to the bistatic cross section. The cross section given in (53) is obtained by Watson–Keller and is identical to Ito's first-order solution. Ito obtained this based on an assumption which corresponds to the diagram shown in figure 5(*c*), where the main point is the conservation of power. The smoothed Bethe–Salpeter equation and our solutions are shown in figures 5(*a*) and (*b*). Our solutions, however, do not conserve the power and higher-order terms must be included in the perturbation expansion to conserve the power. We shall discuss the second-order ladder and cyclic theory including higher-order terms and power conservation in a future paper.

5. Specific intensity at the observation point

We now consider the incoherent specific intensity which gives the power flux density directed in a given direction $\hat{s}$ at a given point r. The specific intensity is determined from the Fourier transform of the mutual coherence function [1] (see figure 8),

$$I(r, \hat{s}) = \int \Gamma_f(r, r') e^{-ikr_d} \, dr_d \tag{55}$$

where $k = k\hat{s}$. We consider a point source $r_0 = r_0'$ ($r_1 = r_1'$), and the exponent in (50) becomes (figure 8)

$$\exp\{ikr_2 - ikr_2'\} = \exp\{ik_0 \cdot r_2 - ik_0' \cdot r_2'\} = \exp\{ik_c \cdot r_d + ik_d \cdot r_c\} \tag{56}$$

where $k_0 = k\hat{o}$, $k_c = \frac{1}{2}(k_0 + k_0')$ and $k_d = k_0 - k_0'$. We take $r_2 = r_2'$ and thus $k_d \perp r_c$. Therefore, we obtain

$$\exp\{ikr_2 - ikr_2'\} = \exp\{ik_c \cdot r_d\}. \tag{57}$$

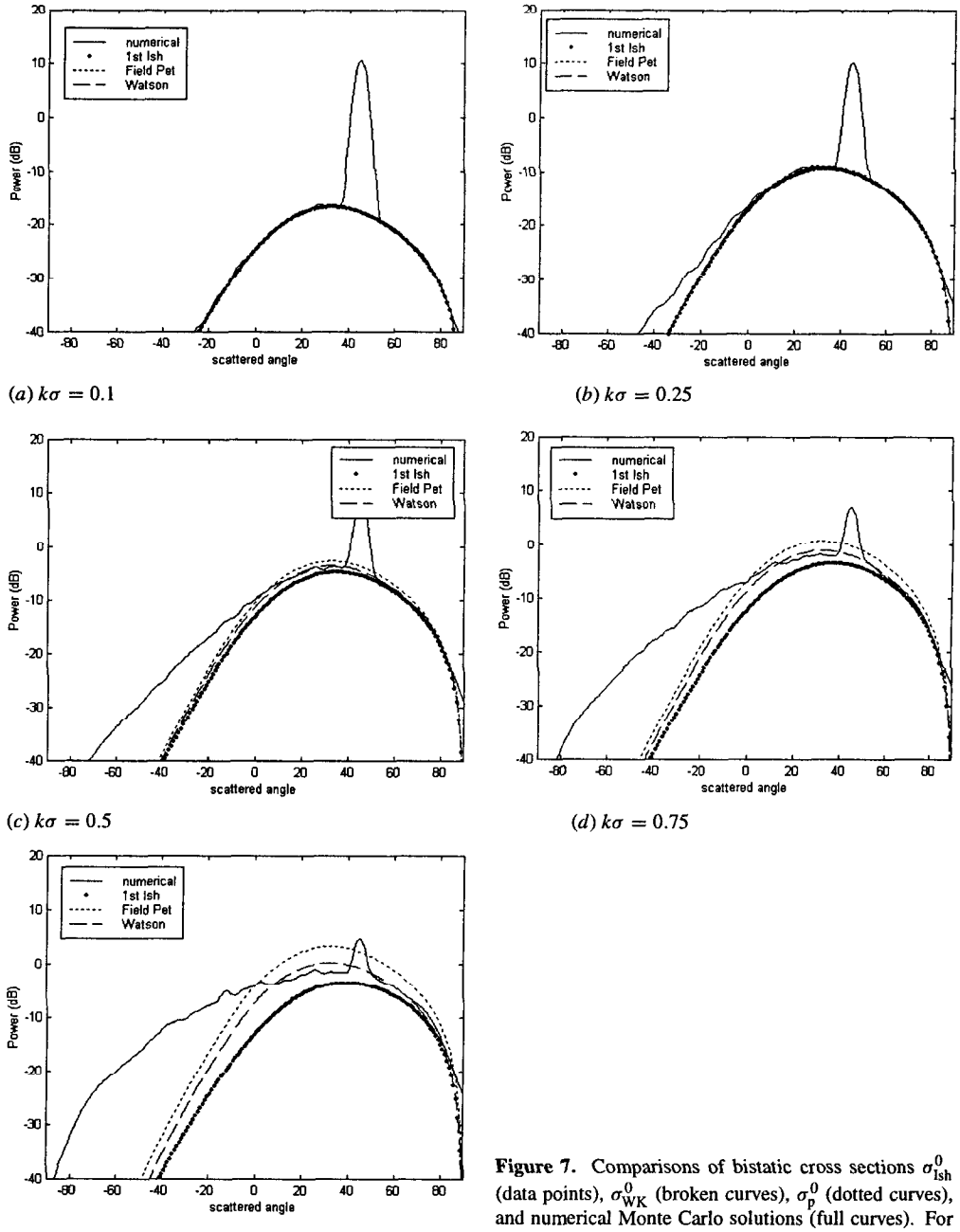

(*a*) $k\sigma = 0.1$

(*b*) $k\sigma = 0.25$

(*c*) $k\sigma = 0.5$

(*d*) $k\sigma = 0.75$

(*e*) $k\sigma = 1.0$

Figure 7. Comparisons of bistatic cross sections σ^0_{Ish} (data points), σ^0_{WK} (broken curves), σ^0_{p} (dotted curves), and numerical Monte Carlo solutions (full curves). For all plots $k_1 = 4.24$ and $\theta_i = 45$ deg.

We can then substitute (50) into (55) and obtain the specific intensity

$$I(r, s) = \int \frac{\mathrm{d}x_{1c}}{2\pi r_2} \sigma^0 (2\pi)^2 \delta(k - k_c) \frac{1}{8\pi k r_1}. \tag{58}$$

Noting that

$$\frac{\mathrm{d}x_{1c} \cos\theta}{r_2} = \mathrm{d}\Omega = \frac{\mathrm{d}k}{k} \tag{59}$$

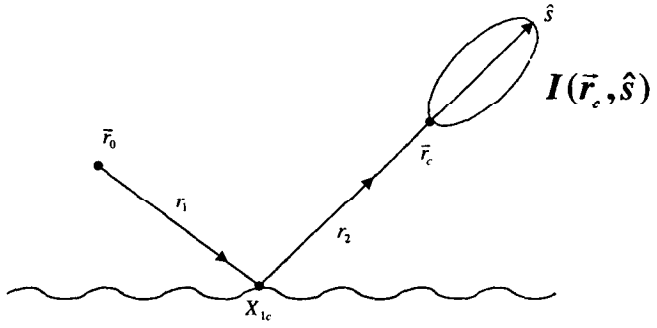

Figure 8. Specific intensity $I(r_c, \hat{s})$.

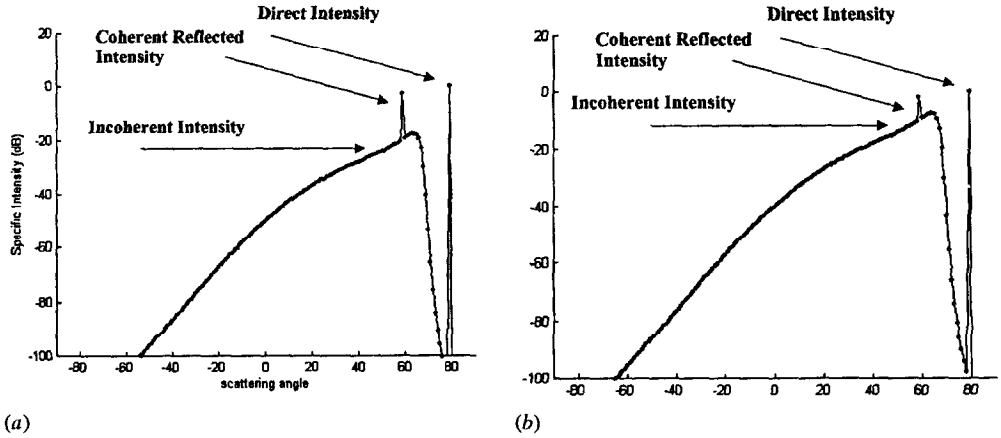

Figure 9. Angular distribution of specific intensity $I(r_c, \hat{s})$. $x_0 = -10\lambda$, $x = 10\lambda$, $z_0 = 4\lambda$, $z = 8\lambda$. (*a*) 1° FOV. (*b*) 10° FOV.

we finally obtain for the specific intensity at a point r_c, in a given direction θ_2

$$I(r, s) = \frac{2\pi}{k \cos\theta_2} \frac{\sigma^0(\theta_1, \theta_2)}{8\pi k r_1}. \tag{60}$$

Figures 9(*a*) and (*b*) show calculations of the specific intensity at an observation point in the forward direction. The specific intensity angular distribution consists of three terms: the direct intensity from the transmitter, the reflected coherent intensity reflected from the rough surface and, finally, the incoherent intensity. Figure 9(*a*) shows the angular distribution for the 1° field-of-view (FOV) arrival into the observation point. The effects of the incoherent intensity are minimal and for a rough surface and object interaction problem, one need only consider the direct and coherent reflected intensity. However, figure 9(*b*) considers a larger FOV. The incoherent intensity is diffused and spreads in angles and therefore the receiver with large FOV has more incoherent intensity than for a smaller FOV receiver. The order of magnitude in the incoherent intensity is comparable to the direct and coherent reflected intensity. Therefore, the incoherent scattering from a rough surface must be carefully considered.

6. Conclusion

This paper presents an analytical theory of the coherent and the incoherent rough surface Green's function for a Dirichlet one-dimensional smooth rough surface. The theory is applicable to surfaces with small RMS height $k\sigma \leqslant 1.0$, but the range of validity is much greater than that of the conventional perturbation method. The coherent Green's function was determined from Dyson's equation, and its spatial Fourier transform representation is given in (23). A saddle-point technique was used to evaluate this expression and is given in (24), (25) and (26). The mutual incoherent function was calculated based on the Bethe–Salpeter equation, and the general solution based on a spatial Fourier transform is given in (45). This is also evaluated using a far-field asymptotic approximation (50). The mutual coherence function was then used to calculate the specific intensity (60). Therefore the theory should be useful for RCS signature related problems and for LGA scattering when both the transmitter and the observation point are close to the surface.

Acknowledgments

The work reported in this paper is supported by ONR (N00014-97-1-0590), ONR (N00014-97-1-0060) and NSF (EC59522031).

References

[1] Ishimaru A 1997 *Wave Propagation and Scattering in Random Media* (Piscataway, NJ: IEEE) and (Oxford: Oxford University Press)

[2] DeSanto J A and Brown G S 1986 Analytical techniques for multiple scattering from rough surfaces *Progress in Optics* vol XXIII, ed E Wolf (Amsterdam: Elsevier) pp 1–62

[3] Bass F G and Fuks I M 1979 *Wave Scattering from Statistically Rough Surfaces* (Oxford: Pergamon)

[4] Barrick D E 1998 Grazing behavior of scatter propagation above rough surface *IEEE Trans. Antennas Propag.* 73–83

[5] Brown G (ed) 1998 Special issue on low-grazing-angle backscattering from rough surfaces *IEEE Trans Antennas Propag.* **46** 1–2

[6] Frisch U 1968 Wave propagation in random media *Probabilistic Methods in Applied Mathematics* ed A T Bharucha-Reid (New York: Academic)

[7] Watson J G and Keller J B 1983 Reflection, scattering and absorption of acoustic waves by rough surfaces *J. Acoust. Soc. Am.* **74** 1887–94

[8] Watson J G and Keller J B 1984 Rough surface scattering via the smoothing method *J. Acoust. Soc. Am.* **75** 1705–8

[9] Ito S 1985 Analysis of scalar wave scattering from slightly rough random surfaces: a multiple scattering theory *Radio Sci.* **20** 1–12

[10] Ishimaru A 1991 *Electromagnetic Wave Propagation, Radiation and Scattering* (New York: Prentice Hall)

[11] Winebrenner D P and Ishimaru A 1985 Application of the phase perturbation techniques to randomly rough surfaces *J. Opt. Soc. Am.* A **2** 2294